Asian Journal of Chemistry; Vol. 30, No. 1 (2018), 97-102

ASIAN JOURNAL OF CHEMISTRY

https://doi.org/10.14233/ajchem.2018.20917

Synthesis of γ-Bi_2MoO_6 by Co-precipitation Method and Evaluation for Photocatalytic Degradation of Rhodamine B, Crystal Violet and Orange II Dyes Under Visible Light Irradiation

LAVAKUSA BANAVATU[1,*], D. SRINIVASA RAO[2] and K. BASAVAIAH[1]

[1]Department of Inorganic and Analytical Chemistry, Andhra University, Visakhapatnam-530 003, India
[2]Department of Physics, V.K.R. College, Budhavaram, Gannavaram-521 101, India

*Corresponding author: E-mail: lavakusa99@gmail.com

Received: 12 July 2017; *Accepted*: 17 October 2017; *Published online*: 30 November 2017; AJC-18658

γ-Bismuth molybdate (γ-Bi_2MoO_6) catalyst has been successfully synthesized by co-precipitation method and followed by calcination using stoichiometry ratio of bismuth nitrate, nitric acid, ammonium molybdate as precursor materials. The synthesized γ-Bi_2MoO_6 nanoparticles characterized by X-ray diffraction for identifying crystalline phases and particle size, Raman spectroscopy identifies active species during the reaction, Fourier transform infrared spectroscopy is to identify adsorbed species and to study the way in which these species are chemisorbed at the surface of the catalyst, UV-visible diffuse reflectance spectroscopy (UV-DRS) revealed for band energy of semiconductors, Field emission scanning electron microscopy (FE-SEM) is to determine morphology and shape of supported particles and Energy dispersive X-ray analysis (EDX) is for elemental analysis of synthesized nanoparticles. The photocatalytic activity of γ–Bi_2MoO_6 catalyst evaluated using the degradation of Rhodamine-B, Crystal Violet and Orange II dyes under visible light irradiation at room temperature.

Keywords: Co-precipitation, Photocatalytic activity, γ-Bi_2MoO_6, Calcination, Visible light irradiation.

INTRODUCTION

Over 70,000 tons of commercial dyes are produced annually for using in textile, paper, leather, pharmaceutical, cosmetic and food industries and an estimated 1-15 % of these dyes make into various aquatic sources as effluents in the form of unused dyes [1]. Several studies indicated that the remnant dyes from a persistent class of health hazards since they are less biodegradable. Photocatalysis utilizes solar energy to decompose harmful dyes, organic and inorganic pollutants present in air and aqueous systems using semiconductors has been the subject of extensive studies as a potential way of solving energy and environmental issues because of their economic and ecologically safe option for solving energy and pollution problems over the past two decades [2-8] or to split water to supply clean and recycle hydrogen energy [9-11]. Most of the investigations have focused on anatase titanium dioxide as the photocatalyst, because of relatively high photocatalytic activity, high chemical stability and inexpensive [12-14]. However, titanium dioxide as a high band gap (~ 3.2 eV) semiconductor and can only be activated by the wavelength in the near ultraviolet region ($\lambda <$ 400 nm) and cannot effectively utilize the major spectrum of sunlight [15,16]. Sunlight is comprised of less than 2 % ultraviolet light. Therefore, the development of a small band energy semiconductor for a visible light photocatalyst consequently has become an imperative topic in current photocatalysis research. Considering the relatively slow reaction rate and poor solar efficiency of TiO_2 which hindered its application, many studies have been carried out to exploit new visible light-driven photocatalysts.

During the past two decades, bismuth molybdates have been received great attention in the field of catalysis and one of the promising visible light driven photocatalytic semiconductor for water splitting and degradation of organic and inorganic pollutants due to their narrow energy gap [17]. Bismuth molybdate has the general chemical formula $Bi_2O_3 \cdot nMoO_3$ where n = 3, 2 or 1 corresponding to α($Bi_2Mo_3O_{12}$), β($Bi_2Mo_2O_9$) and γ(Bi_2MoO_6) phases, respectively. Of these γ-Bi_2MoO_6 phase has excellent intrinsic physical and chemical properties, including ion conduction, dielectric and gas sensing properties [18,19] and also shows excellent catalytic activity towards oxidation of propylene [20], ammoxidation of propene [21]. The structure of γ-Bi_2MoO_6, which is built upon $[Bi_2O_2]^{2+}$ layers alternated with layers of corner sharing MoO_6 octahedra (Aurivillius-type structure) [22]. It results in the photocatalytic activities of Bi_2MoO_6 is larger than that of $Bi_2Mo_3O_{12}$ and $Bi_2Mo_2O_9$.

Bismuth molybdates can be prepared by several methods that include solid state reaction [23], spray drying [24,25], reflux method [26], ultrasonic assisted synthesis [27], hydrothermal synthesis [28,29], co-precipitation method [30] and sol-gel [31], *etc*. Among these methods, many researchers reported the co-precipitation route is one the most effective method for synthesizing bismuth molybdate nanoparticles [32-34]. However, the material synthesized by co-precipitation method at pH 3 [35] for desired phase and characterized by X-ray diffraction (XRD), Raman spectroscopy, Fourier transform infrared spectroscopy (FT-IR), UV-visible diffuse reflectance spectroscopy (UV-DRS), field emission scanning electron microscopy (FE-SEM) and energy dispersive X-ray analysis (EDX). The catalytic activity of synthesized γ-Bi_2MoO_6 nanoparticles evaluated using the photocatalytic degradation of Rhodamine-B, Orange II and Crystal Violet dyes under visible light irradiation at room temperature.

EXPERIMENTAL

Bismuth nitrate [$Bi(NO_3)_3{\cdot}5H_2O$], nitric acid [HNO_3, 78 %], ammonium molybdate [$(NH_4)_6Mo_7O_{24}{\cdot}4H_2O$] and ammonium hydroxide, Crystal Violet, Orange II, Rhodamine-B. All chemicals received from Merck India and used without further purifier.

Synthesis of γ-Bi_2MoO_6: γ-Bi_2MoO_6 catalyst was prepared by a co-preparation method. 4.75 g of bismuth nitrate (0.49 M $Bi(NO_3)_3{\cdot}5H_2O$) was dissolved in 20 mL of diluted nitric acid (1.5 M HNO_3). The solution was then added drop-wise into the aqueous solution containing 0.035 M of ammonium molybdate (0.86 g/20 mL $(NH_4)_6Mo_7O_{24}{\cdot}4H_2O$) under vigorous stirring during the co-precipitation step, pH of the mixed solution was precisely controlled by adjusting the amount of ammonia solution added and kept pH value at 3.0 for formation of the desired phase of γ-Bi_2MoO_6 nanoparticles. The reaction of the solution continuously stirred at room temperature for 8 h and obtained precipitate was filtered, dried and then it was calcined at 475 °C for 5 h to yield the γ-Bi_2MoO_6 nanoparticles [35,36].

Characterization: The crystalline structure of the γ-Bi_2MoO_6 was investigated by powder X-ray diffraction (XRD, PanAlytical, X-Pert pro, Netherland) with CuK_α (l 1.54218 Å) radiation. Fourier transform infrared (IR Prestige21, Shimadzu, Pvt Ltd, Japan) spectra of the sample were recorded on FTIR spectrometer using conventional potassium bromide (KBr) pellets within a wave number range 5000-500 cm^{-1} and Raman spectra (BWTEK MiniRam BTR-111 Miniature Raman Spectrometer) recorded to the Raman shift range 1200-200 cm^{-1}. The size and morphology of the product were obtained with a scanning electron microscope (FE-SEM-CARL Zeiis Germany, Model Ultra 55 FE-SEM, Gemini column, 1nm Resolution, detector is INLENSE), Energy dispersive X-ray analysis EDX (Oxford company, model 20 nm X Ma) UV-visible diuse reflectance spectra of the sample were obtained in the range 300-800 nm using a UV-visible spectrophotometer (UV2550, Shimadzu, Japan) barium sulphate was used as a reflectance standard.

Photocatalytic test: Organic pollutant such as Rhodamine-B, Crystal Violet and Orange II were chosen for photocatalytically evaluate the photocatalytic activities of the as synthesized catalyst. A 400 W HgX lamp was used as the light source to provide the simulated solar light. The experiments performed at an ambient temperature. The photocatalysts (0.05 g) were added into 50 mL of organic pollutant (5 ppm) solution and the suspension was magnetically stirred for 30 min in the dark to reach an adsorption-desorption equilibrium with the photocatalysts. At every 30 min time intervals, a 3 mL of solution collected and then analyzed on UV-visible spectrophotometer during the photodegradation process. The concentration of Rhodamine-B, Crystal Violet and Orange II pollutant (dyes) were determined by monitoring the variations in the main absorption centered at 55, 584 and 485 nm, respectively.

RESULTS AND DISCUSSION

Fig. 1 presents the powder XRD pattern of γ-Bi_2MoO_6 nanoparticles and it shows the characteristic XRD peaks centered at 2θ = 11.01°, 28.4°, 32.8°, 33.3°, 36.2°, 47.3°, 55.8°, 56.4°, 58.6° which can be indexed as (020), (111), (131), (002), (060), (151), (202), (133), (191), (262) planes, respectively. The XRD pattern of γ-Bi_2MoO_6 well agreement with the orthorhombic phase Bi_2MoO_6 (JCPDS card No 72-1574) [37]. No impurities can be found such as secondary phases Bi_2O_3, MoO_3 and others were present in the main product of γ-Bi_2MoO_6 NPs. The high peak suggests that the material is highly crystalline and nanosized. The average crystallite size was calculated from the XRD line boarding using Debye-Scherrer relationship given in the eqn. 1:

$$L = 0.9\lambda/(\beta\cos\theta) \quad (1)$$

where L is the crystallite size, β is the full width at half maximum line width (FWHM) and λ was the wavelength of X-rays. The average crystalline size of the γ-Bi_2MoO_6 calculated from diffraction peaks found to be 43-47.58 nm.

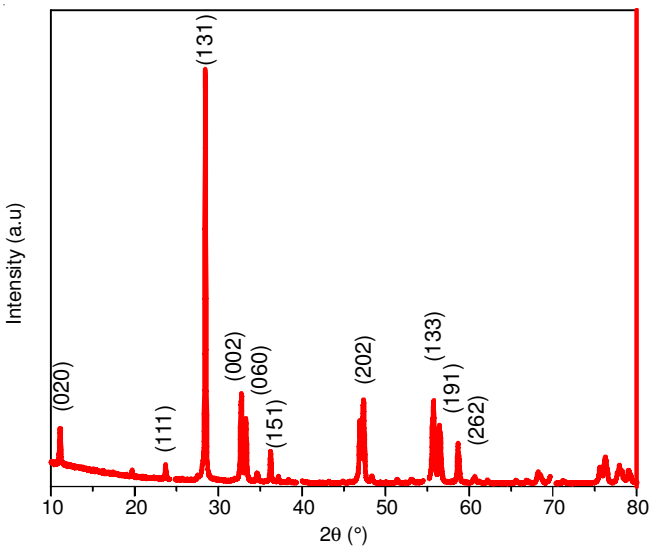

Fig. 1. Powder XRD patterns of γ-Bi_2MoO_6

The lattice parameter of the sample was calculated using the formula given in eqn. 2:

$$Sin^2\theta = \lambda^2 h2/4a^2 + \lambda^2k^2/4b^2 + \lambda^2l^2/4c^2 \quad (2)$$

where h, k and l are Miller's indices. Calculated the lattice parameter from eqn. 2 found to be a = 5.382 Å, b = 16.122 Å and c = 5.401 Å.

The Raman spectra of γ-Bi_2MoO_6 nanoparticles shown in Fig. 2, which correspond well to the result of Raman spectroscopy. The typical vibration bands for the γ-Bi_2MoO_6 sample was observed at 849 cm^{-1} (s), 795 cm^{-1} (vs), 715 cm^{-1} (w), 401 cm^{-1} (vw), 352 cm^{-1} (w), 325 cm^{-1} (vw), 282 cm^{-1} (vs). The vibrational bands 849 cm^{-1}, 795 cm^{-1} (vs) peaks can be ascribed to the stretching modes of Mo-O bonds and vibrational band 715 cm^{-1} (w) peak can be ascribed to the stretching modes of Bi-O/Bi-O-Mo stretching observed. The Raman spectrum of γ-Bi_2MoO_6 phase shows a strong band at 795 cm^{-1}, which is A_{1g} mode and represents the symmetric stretch of the MoO_6 octahedron. The band with strong intensity at 849 cm^{-1} also have A_{1g} character and are due to orthorhombic distortion of the octahedron. The modes between 280 and 360 cm^{-1} have E_g character, plausibly due to the rocking mode of the octahedron [35,38,39].

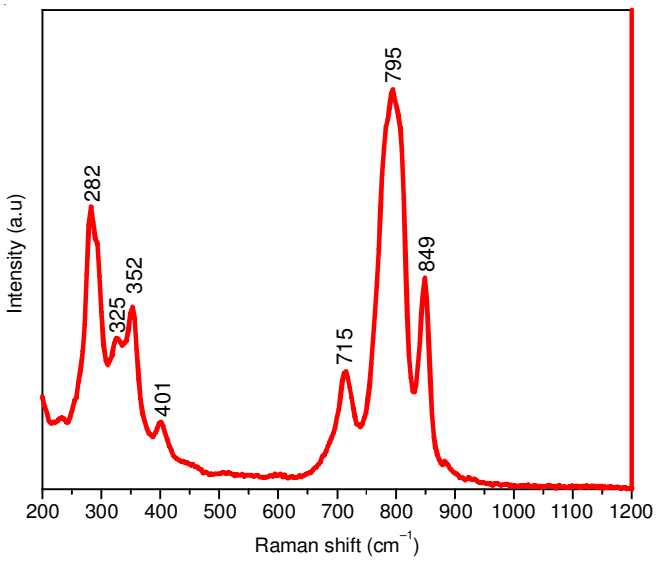

Fig. 2. Raman spectrum of γ-Bi_2MoO_6 nanoparticles

Fig. 3 shows FT-IR spectrum of γ-Bi_2MoO_6 sample. The main absorption bands at 736, 798, 843 cm^{-1} are mainly related to Bi-O and Mo-O stretching modes. Generally the absorption bands between 950-400 cm^{-1} range described to Bi-O and Mo-O stretching and Mo-O-Mo bridging stretching modes [40,41]. The peaks at 1626 and 1383 cm^{-1} in the FT-IR spectrum of the sample are assigned to the vibration of O-H stretching to the adsorbed water molecule to the sample. The peak at 3438 cm^{-1} corresponding to O(2)H···O(6) intramolecular hydrogen bonds to the adsorbed water molecule of the sample [42]. The bands around 843 and 798 cm^{-1} can be assigned as the asymmetric and symmetric stretching modes of MoO_6 involving vibrations of the oxygen atoms, respectively. The band at 736 cm^{-1} can be attributed to the involving to the asymmetric stretching mode MoO_6 involving vibration of the equatorial oxygen atoms [43-45].

The surface morphology of γ-Bi_2MoO_6 nanoparticles was investigated by field emission scanning electron microscopy (FE-SEM). The FE-SEM images of γ-Bi_2MoO_6 is depicted in Fig. 4(a-b) shows that the FE-SEM images of γ-Bi_2MoO_6 nanoparticles clearly observed the hexagonal shapes and with particle size range 47-90 nm. Elemental composition and purity of

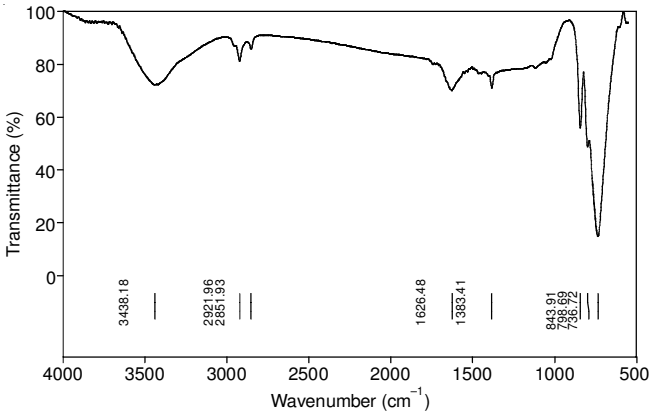

Fig. 3. FTIR spectrum of γ-Bi_2MoO_6 sample synthesized in the co-precipitation method

compound confirmed by energy dispersive X-ray (EDX) analysis. Fig. 4(c) shows the EDX spectrum of γ-Bi_2MoO_6 sample shows the presence of Bi, Mo and O only due to perfect sample synthesized without any other impurities.

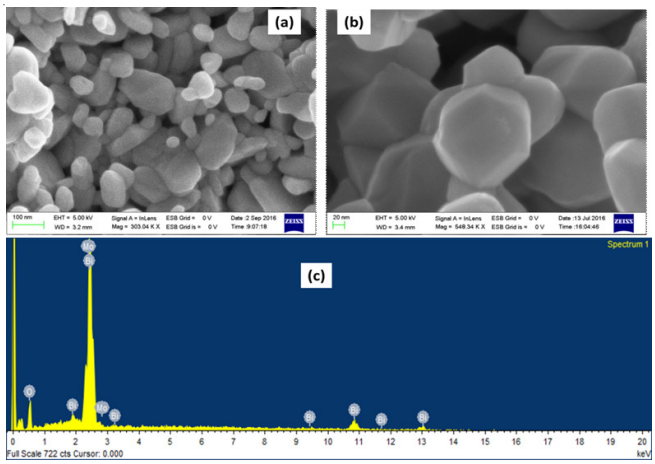

Fig. 4. (a-b) FE-SEM images of γ-Bi_2MoO_6 (c) EDX spectrum of γ-Bi_2MoO_6

Optical properties: Fig. 5 shows the synthesized material and the sample exhibit absorption edge at 499 nm suggests the material, which had photoactive under visible light irradiation does not derive from any impurity level but the steep and shape of the spectra suggests that the light absorption due to a band gap transition and calculated the band from eqn. 3, band gap of the γ-Bi_2MoO_6 nanoparticles is 2.48 eV and band gap compared with that reported by Kudo and Yu [46]. Generally, narrow band gap materials suggest to the good semiconductors were preferred for efficient charge separation, the photocurrent generated by the sample measured which correlates with photocatalytic activity.

$$\text{Band gap energy } (E_g) = h*c/\lambda \quad (3)$$

where E_g, h, c, λ are band gap energy, plank constant, the speed of light, cut off wavelength, respectively.

Photocatalytic effect: General photocatalytic degradation of dyes by a photocatalyst critically depends on particle size, crystallinity, morphology, band gap energy, charge recombination, efficient charge separation and the value of photocurrent indirectly reflects the semiconductor's ability to generate and

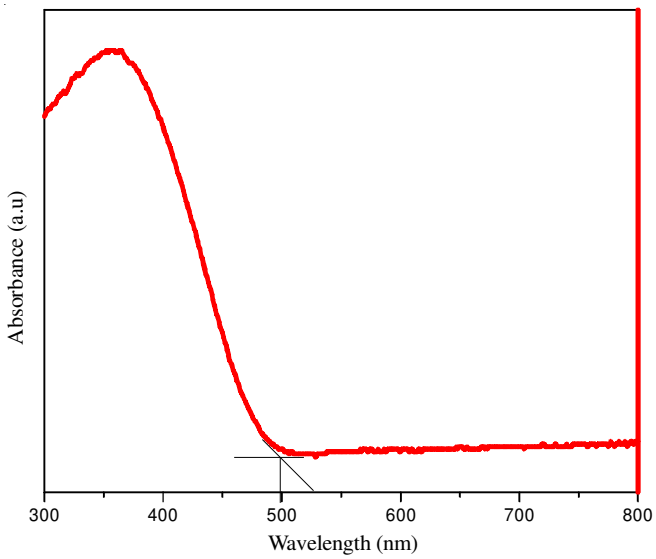

Fig. 5. UV-visible diffuse reflectance spectra of γ-Bi_2MoO_6

transfer a photogenerated charge carrier under irradiation, which correlates with the photocatalytic activity. The γ-Bi_2MoO_6 had good photocatalytic property because XRD revealed nanosized and good crystallinity, FE-SEM revealed hexagonal shape, UV-DRS raveled narrow band gap and good efficiency for charge separation. Fig. 6 shows the photocatalytic activity of as prepared γ-Bi_2MoO_6nanoparticles evaluated under visible light irradiation over degradation of organic pollutant, Rhodamine-B, Orange II and Crystal violet chosen as a representative model pollutant. The establishment of adsorption-desorption equilibrium was obtained under continuous stirring 30 min before the degradation reaction was carried out. Fig. 6(a-c) displays the degradation of Rhodamine-B (Rh-B), Orange II and Crystal violet (CV) evaluated degradation under visible light irradiation measured to UV-visible spectrometer to the cut-off filter 554, 487 and 584 nm, respectively. Fig. 6(d) shows the percentage of photo-catalytic degradation for a different organic pollutant to the function of % of degradation *versus* time (min) and calculated percentage of degradation from eqn. 4. Fig. 6(d) revealed the percentage of degradation of Rhodamine-B, Orange II and Crystal violet with 30 min interval 64.30, 27.92, 31.60 %, respectively, which suggest the γ-Bi_2MoO_6 catalyst more efficiency degradable Rhodamine-B with less

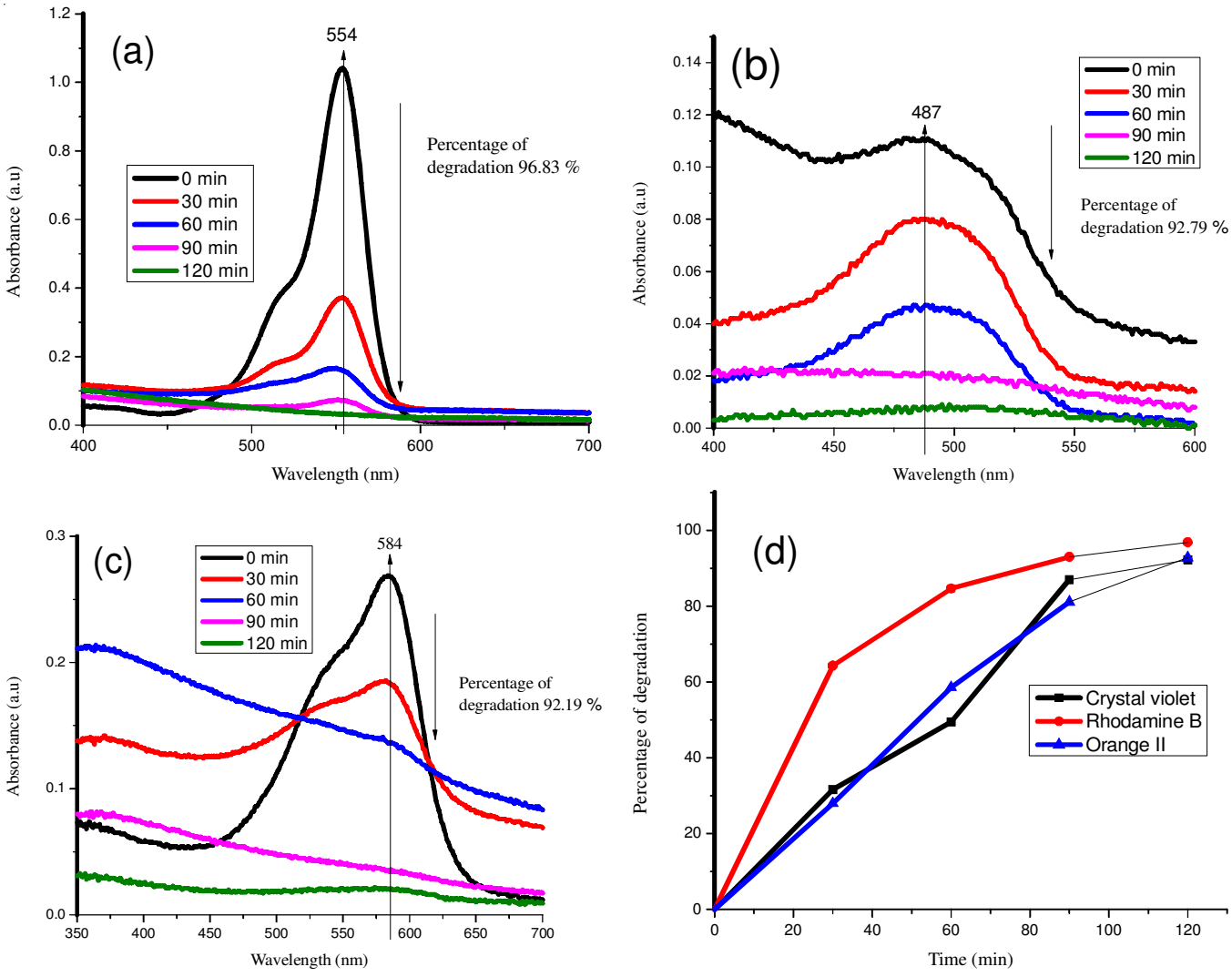

Fig. 6. UV-visible spectra for photocatalytic evolution of organic pollutant (a) Rhodamine-B (b) Orange II (c) Crystal violet (d) Comparison of photocatalytic activity of γ-Bi_2MoO_6 catalyst with different organic pollutant under visible light irradiation as a function of the % of degradation *versus* time

time of interval compared with other pollutant and 120 min time interval degradable of Rhodamine-B, Orange II and Crystal violet 96.83, 92.79, 92.19 %, respectively, which suggest γ-Bi_2MoO_6 catalyst efficiency to degradable of Orange II and Crystal violet pollutants with long time of interval almost nearly equal but efficiency degradable more for Rhodamine-B pollutant, which revealed photocatalytic efficiency of synthesized γ-Bi_2MoO_6 catalyst more favourable for rhodamine B compared with other pollutant Orange II and Crystal violet. Table-1 shows clearly catalytic efficiency of γ-Bi_2MoO_6 different organic pollutant with respect to different time intervals.

$$\text{Degradation } (\%) = \frac{(A_o - A_t)}{A_o} \times 100 \quad (4)$$

where A_o and A_t are, respectively initial absorbance and absorbance at time 't'.

TABLE-1
PERCENTAGE OF ORGANIC POLLUTANT DEGRADABLE WITH RESPECT DIFFERENT TIME INTERVAL

Time (min)	Percentage of degradation		
	Crystal Violet	Rhodamine B	Orange II
0	0	0	0
30	31.59851	64.29942	27.92793
60	49.44238	84.64491	58.55856
90	86.98885	92.99424	81.08108
120	92.19331	96.83301	92.79279

Based on the photocatalytic degradation of organic pollutant (OP) in the solution containing γ-Bi_2MoO_6 (BMO) nanoparticles, a possible mechanism was proposed [47,48]:

$$BMO + hv \rightarrow BMO\ (e_{cb}^-) + BMO\ (h_{vb}^+) \quad (5)$$

$$BMO\ (e_{cb}^-) + O_2 \rightarrow O_{2*}^- + BMO \quad (6)$$

$$OP + hv \rightarrow OP^* \quad (7)$$

$$OP_{ad}^* + BMO \rightarrow OP^{*+} + BMO\ (e_{cb}^-) \quad (8)$$

$$H_2O \text{ or } OH + BMO\ (h_{vb}^+) \rightarrow OH^* \quad (9)$$

$$OP^{*+} + O_2^{*-} \rightarrow \text{Subproducts} \quad (10)$$

Conclusion

γ-Bi_2MoO_6 nanoparticles successfully synthesized by co-precipitation method by controlled specific pH condition and followed by calcination treatment at 475 °C for 5 h. Based on various characterization techniques, the appropriate condition for the synthesis of hexagonal γ-Bi_2MoO_6 nanoparticles was at pH 3. Seen from UV-visible diffuse-reflectance spectroscopy analysis of the prepared samples, the band gap adsorption edge of 499 nm corresponding to the band gap energy to be 2.48 eV. In addition, γ-Bi_2MoO_6 nanoparticles good photocatalytic properties to photodegradation of both cationic dyes (Rhodamine B, Crystal violet) anionic dye (Orange II) at room temperature and more efficiency for photodegradable cationic dyes with short time intervals compare to anionic dyes.

ACKNOWLEDGEMENTS

The authors gratefully acknowledge to University Grant Commission, New Delhi for financial support for this work and DST-FIST Instrument Laboratory, Department of Inorganic & Analytical Chemistry, Andhra University, Visakhapatnam, India.

REFERENCES

1. H. Zollinger, Azo Dyes and Pigments, Colour Chemistry-Synthesis, Properties and Applications of Organic Dyes and Pigments, VCH, New York, pp. 92-100 ((1991).
2. H. Al-Ekabi and N. Serpone, *J. Phys. Chem.*, **92**, 5726 (1988); https://doi.org/10.1021/j100331a036.
3. S. Kutsuna, Y. Ebihara, K. Nakamura and T. Ibusuki, *Atmos. Environ.*, **27**, 599 (1993); https://doi.org/10.1016/0960-1686(93)90217-M.
4. V. Augugliaro, L. Palmisano, M. Schiavello, A. Sclafani, L. Marchese, G. Martra and F. Miano, *Appl. Catal. A*, **69**, 323 (1991); https://doi.org/10.1016/S0166-9834(00)83310-2.
5. O. Legrini, E. Oliveros and A.M. Braun, *Chem. Rev.*, **93**, 671 (1993); https://doi.org/10.1021/cr00018a003.
6. M. Anpo, H. Yamashita, Y. Ichihashi and S. Ehara, J. Electronal. Chem., **396**, 21 (1995); https://doi.org/10.1016/0022-0728(95)04141-A.
7. D.F. Ollis, C.Y. Hsiao, L. Budiam and C.L. Lee, *J. Catal.*, **88**, 89 (1984); https://doi.org/10.1016/0021-9517(84)90053-8.
8. R.W. Matthews, *Sol. Energy*, **38**, 405 (1987); https://doi.org/10.1016/0038-092X(87)90021-1.
9. H. Tong, S. Ouyang, Y. Bi, N. Umezawa, M. Oshikiri and J. Ye, *Adv. Mater.*, **24**, 229 (2012); https://doi.org/10.1002/adma.201102752.
10. P. Wang, B. Huang, X. Qin, X. Zhang, Y. Dai, J. Wei and M.-H. Whangbo, *Angew. Chem. Int. Ed.*, **47**, 7931 (2008); https://doi.org/10.1002/anie.200802483.
11. M. Murdoch, G.I.N. Waterhouse, M.A. Nadeem, J.B. Metson, M.A. Keane, R.F. Howe, J. Llorca and H. Idriss, *Nat. Chem.*, **3**, 489 (2011); https://doi.org/10.1038/nchem.1048.
12. M.R. Hoffmann, S.T. Martin, W. Choi and D.W. Bahnemann, *Chem. Rev.*, **95**, 69 (1995); https://doi.org/10.1021/cr00033a004.
13. K. Honda and A. Fuhishima, *Nature*, **238**, 37 (1972); https://doi.org/10.1038/238037a0.
14. A. Fujishima, T.N. Rao and D.A. Tryk, *J. Photochem. Photobiol. Photochem. Rev.*, **1**, 1 (2000); https://doi.org/10.1016/S1389-5567(00)00002-2.
15. Y. Park, S.H. Lee, S.O. Kang and W. Choi, *Chem. Commun.*, **46**, 2477 (2010); https://doi.org/10.1039/b924829c.
16. D. Kannaiyan, E. Kim, N. Won, K.W. Kim, Y.H. Jang, M.-A. Cha, D.Y. Ryu, S. Kim and D.H. Kim, *J. Mater. Chem.*, **20**, 677 (2010); https://doi.org/10.1039/B917858A.
17. R.E. Newnham, R.W. Wolfe and J.F. Dorrian, *Mater. Res. Bull.*, **6**, 1029 (1971); https://doi.org/10.1016/0025-5408(71)90082-1.
18. P. Tao, Y. Xu, Y. Zhou, C. Song, Y. Qiu, W. Dong, M. Zhang and M. Shao, *Mater. Res.*, **20**, 786 (2017); https://doi.org/10.1590/1980-5373-mr-2016-0824.
19. J. Li, X. Liu, Z. Sun and L. Pan, *Ceramics Int.*, **41**, 8592 (2015); https://doi.org/10.1016/j.ceramint.2015.03.068.
20. A.P. Gorshkov, I.K. Kolchin, A.M. Gribov, L.Ya. Margolis j petroleum chemistry Volume 8, Issue 2 (1968) 118-122.
21. N. Hykaway, W.M. Sears, R.F. Frindt and S.R. Morrison, *Sens. Actuators*, **15**, 105 (1988); https://doi.org/10.1016/0250-6874(88)87001-X.
22. F.R. Theobald, A. Laarif and A.W. Hewat, *Ferroelectrics*, **56**, 219 (1984); https://doi.org/10.1080/00150198408221372.
23. C.S. Guo, J. Xu, S.F. Wang, L. Li, Y. Zhang and X.C. Li, *CrystEngComm*, **14**, 3602 (2012); https://doi.org/10.1039/c2ce06757a.
24. M. Zhang, C. Shao, J. Mu, Z. Zhang, Z. Guo, P. Zhang and Y. Liu, *CrystEngComm*, **14**, 605 (2012); https://doi.org/10.1039/C1CE05974B.
25. S. Williams, M. Puri, A.J. Jacobson and C.A. Mims, *Catal. Today*, **37**, 43 (1997); https://doi.org/10.1016/S0920-5861(96)00258-1.

26. M.T. Le, W.J.M. Van Well, I. Van Driessche and S. Hoste, *Appl. Catal.*, **267**, 227 (2004); https://doi.org/10.1016/j.apcata.2004.03.007.
27. M.T. Le, W.J.M.V. Well, P. Stoltze, I.V. Driessche and S. Hoste, *Appl. Catal.*, **282**, 189 (2005); https://doi.org/10.1016/j.apcata.2004.12.010.
28. Y. Shimodaira, H. Kato, H. Kobayashi and A. Kudo, *J. Phys. Chem. B*, **110**, 17790 (2006); https://doi.org/10.1021/jp0622482.
29. L. Zhou, W. Wang and L. Zhang, *J. Mol. Catal. A*, **268**, 195 (2007); https://doi.org/10.1016/j.molcata.2006.12.026.
30. A.M. Beale and G. Sankar, *Chem. Mater.*, **15**, 146 (2003); https://doi.org/10.1021/cm020463z.
31. M.T. Le, L.H. Bac, I. Van Driessche, S. Hoste and W.J.M. Van Well, *Catal. Today*, **131**, 566 (2008); https://doi.org/10.1016/j.cattod.2007.10.038.
32. A. Martínez-de la Cruz and S. Obregón Alfaro, *J. Mol. Catal. Chem.*, **320**, 85 (2010); https://doi.org/10.1016/j.molcata.2010.01.008.
33. E. Luévano-Hipólito, A.M. Cruz and E.L. Cuéllar, *J. Taiwan Inst. Chem. Eng.*, **45**, 2749 (2014); https://doi.org/10.1016/j.jtice.2014.05.024.
34. E. Luévano-Hipólito, A.M. Cruz, Q.L. Yu and H.J.H. Brouwers, *Appl. Catal. A*, **468**, 322 (2013); https://doi.org/10.1016/j.apcata.2013.09.013.
35. J.C. Jung, H. Kim, A.S. Choi, Y.M. Chung, T.J. Kim, S.J. Lee, S.H. Oh and I.K. Song, *J. Mol. Catal. Chem.*, **259**, 166 (2006); https://doi.org/10.1016/j.molcata.2006.06.022.
36. W.J.M. van Well, M.T. Le, N.C. Schiodt, S. Hoste and P. Stoltze, *J. Mol. Catal. Chem.*, **256**, 1 (2006); https://doi.org/10.1016/j.molcata.2006.04.030.
37. T. Zhang, J. Huang, S. Zhou, H. Ouyang, L. Cao and A. Li, *Ceramics Int.*, **39**, 7391 (2013); https://doi.org/10.1016/j.ceramint.2013.02.079.
38. Y.H. Shi, S.H. Feng and C.S. Cao, *Mater. Lett.*, **44**, 215 (2000); https://doi.org/10.1016/S0167-577X(00)00030-6.
39. R. Murugan, *Phys B*, **352**, 227 (2004); https://doi.org/10.1016/j.physb.2004.07.015.
40. A. Phuruangrat, P. Jitrou, P. Dumrongrojthanath, N. Ekthammathat, B. Kuntalue, S. Thongtem and T. Thongtem, *J. Nanomater.*, **Article ID 789705** (2003); https://doi.org/10.1155/2013/789705.
41. L.M. Thang, Ph.D. Thesis, Synthesis and Application of Bismuth Molybdates, Ghent University, Gent, Belgium (2005).
42. F.D. Hardcastle and E.I. Wachs, *J. Phys. Chem.*, **95**, 5031 (1991); https://doi.org/10.1021/j100166a025.
43. P. Graves, G. Hua and S. Myhra and J.G. Thompson, *J. Solid State Chem.*, **114**, 112 (1995); https://doi.org/10.1006/jssc.1995.1017.
44. K. Tashiro and M. Kobayashi, *Polymer*, **32**, 1516 (1991); https://doi.org/10.1016/0032-3861(91)90435-L.
45. D. Chen, Q. Hao, Z. Wang, H. Ding and Y. Zhu, *CrystEngComm*, **18**, 1976 (2016); https://doi.org/10.1039/C6CE00264A.
46. J. Yu and A. Kudo, *Chem. Lett.*, **34**, 1528 (2005); https://doi.org/10.1246/cl.2005.1528.
47. B. Cheng, W. Wang, L. Shi, J. Ran and H. Yu, *Int. J. Photoenergy*, **Article ID 797968** (2012); https://doi.org/10.1155/2012/797968.
48. Y. Zheng, F. Duan, J. Wu, L. Liu, M. Chen and Y. Xie, *J. Mol. Catal. A*, **303**, 9 (2009); https://doi.org/10.1016/j.molcata.2008.12.010.